

# Alloy broadening of the transition to the non-trivial topological phase of $\text{Pb}_{1-x}\text{Sn}_x\text{Te}$

A. Łusakowski and T. Story

*Institute of Physics, Polish Academy of Sciences, Al. Lotników 32/46, 02-668 Warsaw, Poland*

P. Bogusławski

*Institute of Physics, Polish Academy of Sciences,  
Al. Lotników 32/46, 02-668 Warsaw, Poland and*

*Institute of Physics, University of Bydgoszcz, ul. Chodkiewicza 30, 85-072 Bydgoszcz, Poland*

Transition between the topologically trivial and non-trivial phase of  $\text{Pb}_{1-x}\text{Sn}_x\text{Te}$  alloy is driven by the increasing content  $x$  of Sn, or by the hydrostatic pressure for  $x < 0.3$ . We show that a sharp border between these two topologies exists in the Virtual Crystal Approximation only. In more realistic models, the Special Quasirandom Structure method and the supercell method (with averaging over various atomic configurations), the transitions are broadened. We find a surprisingly large interval of alloy composition,  $0.3 < x < 0.6$ , in which the energy gap is practically vanishing. A similar strong broadening is also obtained for transitions driven by hydrostatic pressure. Analysis of the band structure shows that the alloy broadening originates in splittings of the energy bands caused by the different chemical nature of Pb and Sn, and by the decreased crystal symmetry due to spatial disorder. Based on our results of *ab initio* and tight binding calculations for  $\text{Pb}_{1-x}\text{Sn}_x\text{Te}$  we discuss different criteria of discrimination between trivial and nontrivial topology of the band structure of alloys.

## I. INTRODUCTION

IV-VI compounds and their substitutional alloys constitute the most important family of topological crystalline insulators. They comprise in particular PbTe and SnTe, which differ by the order of levels at the L point of the Brillouin Zone (BZ): in PbTe, the symmetry of the valence band maximum, VBM, (conduction band minimum, CBM) is  $L_{6+}$  ( $L_{6-}$ ), while in the topologically non-trivial SnTe the order is inverted, which is referred to as the inverted band structure with a negative energy gap  $E_{gap}$ . We stress that a negative gap still means an insulating situation with the open gap  $|E_{gap}| > 0$ . An analogous situation occurs for the second pair of IV-VI compounds, PbSe and SnSe.<sup>1,2</sup> Pseudobinary alloys of those compounds offer a unique possibility of detailed studies of the transition between topologically trivial and nontrivial phases. Such studies were performed for the  $\text{Pb}_{1-x}\text{Sn}_x\text{Se}$  alloy. In this case, Angle Resolved Photoemission Spectroscopy data showed that in the relatively wide composition window  $0.2 < x < 0.4$  the transition to the nontrivial phase is driven by the decreasing temperature.<sup>3-6</sup> It is believed that the observed inversion of the band gap character is mainly induced by the decrease of the lattice constant due to thermal contraction. This premise is supported both by the experimental pressure dependencies of the lead and tin chalcogenides band gaps<sup>1,2</sup> and by theoretical analysis.<sup>7</sup>

Previous theoretical studies of IV-VI alloys were mostly conducted within the Virtual Crystal Approximation (VCA), which essentially leads to almost linear dependencies of alloy properties on composition. VCA explained a number of important features observed in experiment, such as the existence of zero gap Dirac-like surface states in thick slabs.<sup>8-10</sup> As we show, the VCA applied to the  $\text{Pb}_{1-x}\text{Sn}_x\text{Te}$  alloy predicts a sharp transition

between the topologically trivial and nontrivial phases driven by the increasing content of Sn, or by the applied hydrostatic pressure (i.e., by the decreasing lattice parameter). One should notice, however, that within the VCA an alloy has the full point and translational symmetry of the rock salt structure. On the other hand, in real alloys there always is the chemical disorder, and those symmetries are missing.

Our goal is to examine to what extent the results of the VCA for  $\text{Pb}_{1-x}\text{Sn}_x\text{Te}$  are realistic. We compare the VCA results with the band structures obtained within supercell models of  $\text{Pb}_{1-x}\text{Sn}_x\text{Te}$  alloy which explicitly differentiate the two cations, Pb and Sn. We show that the presence of two types of cations together with alloy randomness drastically modifies the band structure. In contrast to the VCA predictions, the dependence of  $E_{gap}$  on the composition is non-linear. Instead of the sharp transition from the direct to the inverted structure, there is a wide composition range  $0.3 < x < 0.5$  with the zero band gap. For the sake of simplicity, in the following the case with the  $E_{gap}$  below 3 meV is referred to as the zero gap case. A similar anomaly characterizes also the pressure induced transition to the non-trivial phase, which can take place for Pb-rich  $\text{Pb}_{1-x}\text{Sn}_x\text{Te}$  with  $x < 0.3$ , when  $E_{gap} > 0$ . With the decreasing lattice constant the energy gap becomes negative, and the band structure inverted. However, in contrast to the VCA prediction of a sharp transition, there is a finite range of pressures (or lattice constants) in which the band gap vanishes.

Analysis of the band structure is obscured by the fact that there is no clear criterion which determines the sign of  $E_{gap}$ , i.e., of the (non)trivial topological character of the alloy. Actually, such a distinction is not obvious even for PbTe and SnTe (or PbSe and SnSe). Indeed, the criterion based on the  $Z_2$  topological index, suitable for systems with topological protection by time reversal sym-

metry, suggests triviality of both compounds. This feature is due to a peculiarity of the band structure with the direct gaps located at four nonequivalent  $L$  points in the BZ. To properly characterize these compounds, another topological index, the mirror Chern number (MCN), was invoked.<sup>11</sup> The MCN can be calculated only for systems with mirror symmetry planes, what is satisfied for the (110) planes of the rock-salt structure, and in the average sense in IV-VI alloys  $\text{Pb}_{1-x}\text{Sn}_x\text{Te}$ .<sup>12</sup> Recently, we showed that also the spin Chern number<sup>13</sup> (SCN) allows to distinguish between the topology of  $\text{PbTe}$  and  $\text{SnTe}$ .<sup>14</sup> Contrary to the MCN, the SCN has a much broader range of applicability, because it can be calculated for crystals with the translational symmetry but without the point symmetry, such as random alloys models of  $\text{Pb}_{1-x}\text{Sn}_x\text{Te}$  considered in the present paper.

The anomalies found for the pressure dependence of  $E_{gap}$  of  $\text{Pb}_{1-x}\text{Sn}_x\text{Te}$  are reflected also in the MCN and SCN, which in the window of lattice constant  $a$  of the vanishing energy gap assume almost random, highly non-monotonic values, and can even vanish in the cases which we would classify as the topologically non-trivial, i. e., with non-positive energy gap. Due to all that, and this is one of the conclusions of the paper, it turns out that in most cases single calculations for a sample with a given tin's concentration and the spatial distribution of cations cannot give the unique answer to the question of positivity or negativity of the energy gap. A simple way, and actually the only one we know, to uniquely determine the sign of the calculated energy gap, and the topological triviality, is to repeat calculations for different lattice constants.

In the next Section, technical details of the calculations are presented. Band structure, wave functions, MCN, and SCN as functions of the lattice constant for pure  $\text{PbTe}$  are analyzed in Section III. We also extend the analysis to  $\text{Pb}_{1-x}\text{Sn}_x\text{Te}$  within the VCA, and show that a sharp topological transition as a function of the composition  $x$  takes place. Section IV is devoted to more realistic models of  $\text{Pb}_{1-x}\text{Sn}_x\text{Te}$  mixed crystals. The topological indices are calculated for 8 and 16 atom supercells. We show that the presence of two different atomic species, Pb and Sn, leads to additional splittings of the energy bands and to significantly different behavior comparing to the VCA description. The dependence of  $E_{gap}$  on the composition for larger supercells is studied using the Special Quasirandom Structures (SQS) method.<sup>15</sup> Section V concludes the paper.

## II. TECHNICAL DETAILS OF CALCULATIONS

### A. Density Functional Theory calculations

We use the open-source OpenMX package for DFT calculations<sup>16</sup> with fully relativistic pseudopotentials. The calculations are done using Ceperly-Alder<sup>17</sup> LDA exchange-correlation functional. For Sn, we use the

original pseudopotentials distributed with OpenMX. The pseudopotentials for Pb and Te with four and six valence electrons, respectively, were generated using the program ADPACK distributed with the OpenMX package. The input parameters for Pb and Te were described in Ref. 18. The reason for generating new pseudopotentials was twofold. First, to properly study the band structure of alloys we must employ large supercells. The pseudopotentials distributed with OpenMX package were generated assuming 14 and 16 valence electrons for Pb and Te, respectively. Thus, to reduce the computational time we generate pseudopotentials with lower numbers of valence electrons. The second reason is more important from the physical point of view. As it is well known the local density approximation underestimates energy gaps. This fact is particularly important for compounds containing heavy elements like  $\text{PbTe}$ . Due to the strong spin-orbit interaction for  $p(\text{Pb})$  orbitals, their energy levels are lower than those of  $5p(\text{Te})$ , what results in the inverted band structure. This problem was discussed in Ref. 18, and solved by a proper adjustment of the spin-orbit coupling for Pb. Here, we use this approach.

### B. Calculations of the Chern Numbers

The prescription for calculation of the SCN for systems where spin is not a good quantum number is presented in the paper by Prodan.<sup>13</sup> He proposed to consider an operator

$$Q(\mathbf{k}) = P(\mathbf{k})\Sigma P(\mathbf{k}), \quad (1)$$

where  $P(\mathbf{k})$  is the projection operator on the valence band states subspace and  $\Sigma$  is the  $z$ -th component of the spin operator. The numerical procedure for calculation of the Chern number is clearly described in Ref. 19, and the method of obtaining both SCN and MCN is presented in Ref. 13. However, because in our calculations the atomic pseudoorbitals on different lattice sites are not orthonormal (what is the case in most tight binding calculations), certain technical points should be explained.

In the tight binding approximation (TBA) the Bloch wave functions  $\psi_{\mathbf{k}n}(\mathbf{r})$  for a given wavevector  $\mathbf{k}$  and the band index  $n$

$$\psi_{\mathbf{k}n}(\mathbf{r}) = \sum_{\alpha=1}^M a_{\mathbf{k}n\alpha} \chi_{\mathbf{k}\alpha}(\mathbf{r}), \quad (2)$$

where  $a_{\mathbf{k}n\alpha}$  are complex coefficients and  $M$  functions

$$\chi_{\mathbf{k}\alpha}(\mathbf{r}) = \frac{1}{\sqrt{N}} \sum_{\mathbf{R}} e^{i\mathbf{k}\mathbf{R}} \varphi_{\alpha}(\mathbf{r} - \mathbf{R} - \boldsymbol{\tau}_{\alpha}) \quad (3)$$

constitute the basis. In Eq. (3)  $\alpha$  denotes the type of spinorbital ( $s$ ,  $p$ ,  $d$  ..., spin direction),  $\mathbf{R}$  numerates the positions of  $N$  elementary cells and  $\boldsymbol{\tau}_{\alpha}$  is a vector describing the center of the spinorbital  $\alpha$  in a cell  $\mathbf{R}$ . The

functions  $\chi_{\mathbf{k}\alpha}(\mathbf{r})$  are not orthonormal:

$$\begin{aligned} & \langle \chi_{\mathbf{k}\alpha} | \chi_{\mathbf{k}\beta} \rangle \equiv S_{\alpha\beta}(\mathbf{k}) \\ & = \sum_{\mathbf{R}} e^{i\mathbf{k}\mathbf{R}} \int d\mathbf{r} \varphi_{\alpha}(\mathbf{r} - \boldsymbol{\tau}_{\alpha}) \varphi_{\beta}(\mathbf{r} - \mathbf{R} - \boldsymbol{\tau}_{\beta}). \end{aligned} \quad (4)$$

As a consequence, the coefficients  $a_{\mathbf{k}n\alpha}$  are calculated not from a simple eigenproblem, but from the generalized eigenproblem:

$$H_{\alpha\beta}(\mathbf{k}) a_{\mathbf{k}n\beta} = E_{\mathbf{k}n} S_{\alpha\beta}(\mathbf{k}) a_{\mathbf{k}n\beta}, \quad (5)$$

where the Hamiltonian  $H_{\alpha\beta}$  is in the basis of functions  $\chi_{\mathbf{k}\alpha}(\mathbf{r})$  and the summation over  $\beta$  is implied.

The periodic part of the Bloch wave function reads

$$u_{\mathbf{k}n}(\mathbf{r}) = \frac{1}{\sqrt{N}} \sum_{\mathbf{R}\alpha} e^{i\mathbf{k}(\mathbf{R}-\mathbf{r})} a_{\mathbf{k}n\alpha} \varphi_{\alpha}(\mathbf{r} - \mathbf{R} - \boldsymbol{\tau}_{\alpha}). \quad (6)$$

The method proposed in Ref. 19 requires the knowledge of matrix elements  $\langle u_{\mathbf{k}n} | u_{\mathbf{k}_1 m} \rangle$ . Simple calculations lead to the following expression

$$\langle u_{\mathbf{k}n} | u_{\mathbf{k}_1 m} \rangle = \sum_{\alpha\alpha_1} a_{\mathbf{k}n\alpha}^* a_{\mathbf{k}_1 m\alpha_1} \quad (7)$$

$$\sum_{\mathbf{R}} \int d\mathbf{r} e^{i(\mathbf{k}-\mathbf{k}_1)\mathbf{r} + i\mathbf{k}_1\mathbf{R}} \varphi_{\alpha}(\mathbf{r} - \boldsymbol{\tau}_{\alpha}) \varphi_{\alpha_1}(\mathbf{r} - \mathbf{R} - \boldsymbol{\tau}_{\alpha_1}).$$

Assuming that the modulus of  $\boldsymbol{\Delta} = \mathbf{k} - \mathbf{k}_1$  is small, this expression may be approximated by

$$\begin{aligned} & \langle u_{\mathbf{k}n} | u_{\mathbf{k}+\boldsymbol{\Delta}m} \rangle \approx \\ & \sum_{\alpha\beta} a_{\mathbf{k}n\alpha}^* (S_{\alpha\beta}(\mathbf{k} + \boldsymbol{\Delta}) + i\Delta_i Z_{\alpha\beta}^i(\mathbf{k} + \boldsymbol{\Delta})) a_{\mathbf{k}+\boldsymbol{\Delta}m\beta} \end{aligned} \quad (8)$$

where

$$Z_{\alpha\beta}^i(\mathbf{k}) = \sum_{\mathbf{R}} e^{i\mathbf{k}\mathbf{R}} \int d\mathbf{r} \varphi_{\alpha}(\mathbf{r} - \boldsymbol{\tau}_{\alpha}) r_i \varphi_{\beta}(\mathbf{r} - \mathbf{R} - \boldsymbol{\tau}_{\beta}). \quad (9)$$

The formula (8) may be directly applied to the calculations of the Chern number for a chosen two dimensional plane in the reciprocal space according to the prescription proposed in Ref. 19. However, in the present paper we calculate both SCN and the MCN what requires additional steps.

Using the Cholesky factorization the overlap matrix  $S_{\alpha\beta}(\mathbf{k})$  can be expressed as the product of two matrices

$$S_{\alpha\beta}(\mathbf{k}) = U_{\alpha\gamma}^{\dagger}(\mathbf{k}) U_{\gamma\beta}(\mathbf{k}), \quad (10)$$

where the matrix  $U_{\alpha\beta}(\mathbf{k})$  is the upper triangular matrix. Using this matrix, for each  $\mathbf{k}$  one finds a new set of basis functions

$$\zeta_{\mathbf{k}\alpha}(\mathbf{r}) = \chi_{\mathbf{k}\beta}(\mathbf{r}) U_{\beta\alpha}^{-1}(\mathbf{k}), \quad (11)$$

which are orthonormal,  $\langle \zeta_{\mathbf{k}\alpha} | \zeta_{\mathbf{k}\beta} \rangle = \delta_{\alpha\beta}$ . In this basis we have to solve a simple eigenvalue problem

$$\tilde{H}_{\alpha\beta}(\mathbf{k}) c_{\mathbf{k}n\beta} = E_n(\mathbf{k}) c_{\mathbf{k}n\alpha}, \quad (12)$$

where

$$\tilde{H}_{\alpha\beta}(\mathbf{k}) = (U^{\dagger}(\mathbf{k}))_{\alpha\gamma}^{-1} H_{\gamma\delta}(\mathbf{k}) U_{\delta\beta}^{-1}(\mathbf{k}) \quad (13)$$

and the eigenvectors are normalized

$$c_{\mathbf{k}n\alpha}^* c_{\mathbf{k}m\alpha} = \delta_{mn}. \quad (14)$$

The following steps are based on the paper by Prodan.<sup>13</sup> We focus on the SCN, and for the MCN the steps are analogous. We construct the projection operator on the valence band states in the  $\zeta$  basis

$$\tilde{P}_{\alpha\beta}(\mathbf{k}) = \sum_{n=1}^{N_v} c_{\mathbf{k}n\alpha} c_{\mathbf{k}n\beta}^*, \quad (15)$$

where  $N_v$  is the number of valence band states.

The matrix of the  $z$ -th component of the spin operator in the basis  $\chi$  reads

$$\Sigma_{\alpha\beta}(\mathbf{k}) = S_{\alpha\gamma}(\mathbf{k}) \Sigma_{\gamma\beta}^0, \quad (16)$$

where  $\Sigma_{\alpha\beta}^0$  is the diagonal matrix with values  $\pm 1$ , depending on the spin of the  $\alpha$ -th spinorbital, Eq. (3). After transforming the above operator to the  $\zeta$  basis,  $\tilde{\Sigma}$ , we construct the operator

$$\tilde{Q}_{\alpha\beta} = \tilde{P}_{\alpha\gamma} \tilde{\Sigma}_{\gamma\delta} \tilde{P}_{\delta\beta}. \quad (17)$$

The matrix  $\tilde{Q}_{\alpha\beta}$  has three groups of eigenvalues. There are  $M - N_v$  vanishing eigenvalues, which correspond to the conduction band states. Among the remaining  $N_v$  eigenvalues,  $N_v/2$  are positive and  $N_v/2$  negative. For each  $\mathbf{k}$  we take eigenvectors corresponding to positive (negative) eigenvalues and we calculate  $C_{s+}$  ( $C_{s-}$ ) SCN.

### C. Projection on the Anion Orbitals

The transition from the topologically trivial to nontrivial phase is closely related to the content of anion  $p$  orbitals in the wave functions from the VBM. In the TBA, the wave functions are build from the spinorbitals of the atoms constituting the supercell (see equations (2) and (3)). From the output of the calculations it is possible to draw out the complex coefficients  $a_{\mathbf{k}n\alpha}$ , which describe the wave function in the TBA for a given wavevector  $\mathbf{k}$  in the  $n$ -th band. The content of anion  $p$  orbitals is defined as

$$C_{Te} = \sum_{\alpha n} |a_{\mathbf{k}n\alpha}|^2 \quad (18)$$

where the sum over  $\alpha$  runs over the anion  $p$  spinorbitals.

The wavevector  $\mathbf{k}$  corresponds to the point in the BZ, where the main energy gap is located. For example, in the case of the  $2 \times 2 \times 2$  supercell the main energy gap is located at  $\mathbf{k} = 0$  of the "folded" BZ. The sum over  $n$  takes into account the two top valence bands. In an analogous way the contents of cation  $p$  orbitals,  $C_{Pb}$  and  $C_{Sn}$ , can be defined.

In the case of pure PbTe where the symmetry of the wave functions of the top valence band is  $L_{6+}$  the value of  $C_{Te}$  is nonzero while for SnTe  $C_{Te}=0$  because the corresponding wave functions are of  $L_{6-}$  symmetry and do not contain anion  $p$  spinorbitals. Results of numerous calculations for the  $2 \times 2 \times 2$  supercells for  $Pb_{1-x}Sn_xSe$  clearly indicate that the analogous results hold for alloys, despite the fact that such crystals, in general, do not have the cubic symmetry. Comparing the values of  $C_{Te}$  with the analysis of the energy gap as a function of the lattice constant we get the result that for a trivial insulator  $C_{Te}$  is about 1.7 while for a nontrivial one it almost vanishes. Because we use OpenMX program with the wave functions basis consisting of atomic non orthonormal pseudoorbitals, the coefficients  $a_{kn\alpha}$  are not normalized to unity and this is why the value of  $C_{Te}$  depends on the size of the supercell. For example, for a 64 atom supercell it is 1.7, while for the 2 atom cell it is about 1.5. Our proposition is that the dependence of  $C_{Te}$  on the lattice constant may determine the topological triviality or nontriviality of the given disordered system. The main advantage of using  $C_{Te}$  is that it can be calculated relatively quickly compared to the calculations of SCN or MCN, which are very time consuming for larger systems.

### III. SYSTEMS WITH THE $O_h$ SYMMETRY

#### A. PbTe

As it was already mentioned, the energy gap of PbTe decreases with the decreasing lattice constant, as it is shown in Fig. 1a. The band gap vanishes for  $a/a_0 \approx 0.971$ , where  $a_0 = 6.46 \text{ \AA}$  is the equilibrium lattice constant of PbTe. With the further decrease of the lattice constant it re-opens as negative.

The transition from positive to negative energy gap coincides with the jump of  $C_{Te}$  from 1.5 to approximately zero, see Fig. 1b. For all values of the lattice constants we calculated the MCN for the (110) plane, and the results are shown in Fig. 1c. The SCN, like the MCN, can be calculated only for two-dimensional plane with periodic boundary conditions. Let  $\mathbf{b}_1$ ,  $\mathbf{b}_2$  and  $\mathbf{b}_3$  be reciprocal lattice vectors which span the primitive PbTe cell in the reciprocal space. For a given  $0 \leq z \leq 1$  let us consider the points

$$\mathbf{p}(z) = x\mathbf{b}_1 + y\mathbf{b}_2 + z\mathbf{b}_3 \quad (19)$$

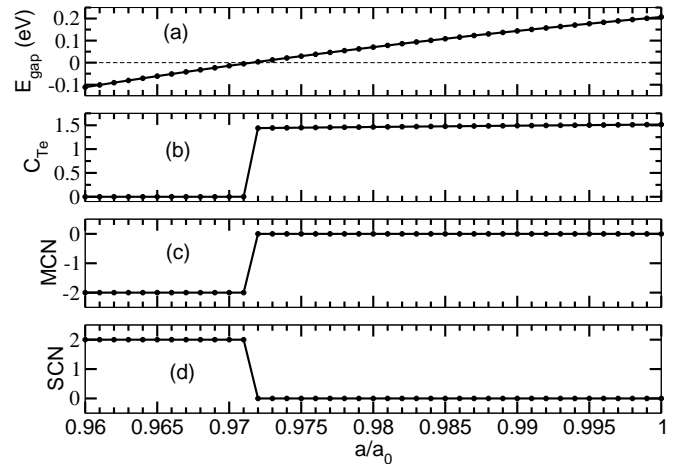


FIG. 1. Lattice constant dependence of (a) the PbTe band gap, (b) parameter  $C_{Te}$  and topological indices (c) MCN, and (d) SCN.

where  $0 \leq x, y \leq 1$ . For this parallelogram we can calculate the  $z$ - dependent SCN.

The results for  $z = 0$  are presented in Fig. 1d. Let us notice that the parallelogram for  $z = 0$  crosses two  $L$  points in the Brillouin zone. The results presented in Fig. 1 are consistent with the presence of surface gapless states. In Fig. 2 we show the energy levels along the  $\bar{X} \rightarrow \bar{\Gamma}$  direction of the reduced two dimensional BZ of the PbTe layer grown along the [001] direction and 200 monolayers thick. We see that the bulk - boundary correspondence theorem is satisfied.

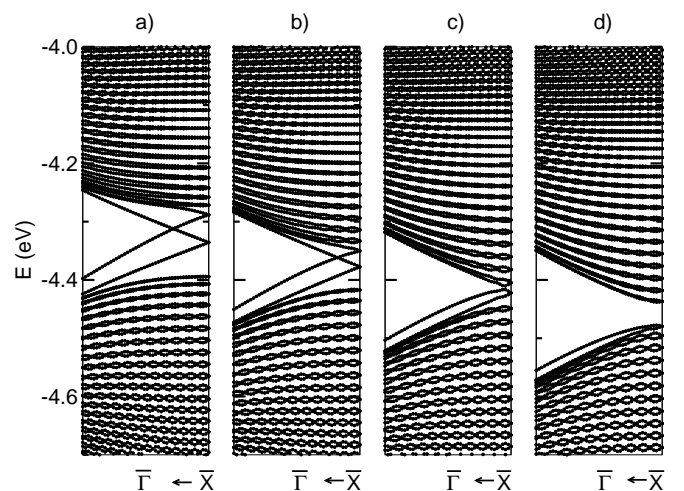


FIG. 2. Energy levels for a 200-atom PbTe layer oriented in the [001] direction for different lattice constant: (a)  $a/a_0 = 0.960$ , (b)  $a/a_0 = 0.965$ , (c)  $a/a_0 = 0.970$  and (d)  $a/a_0 = 0.975$ .

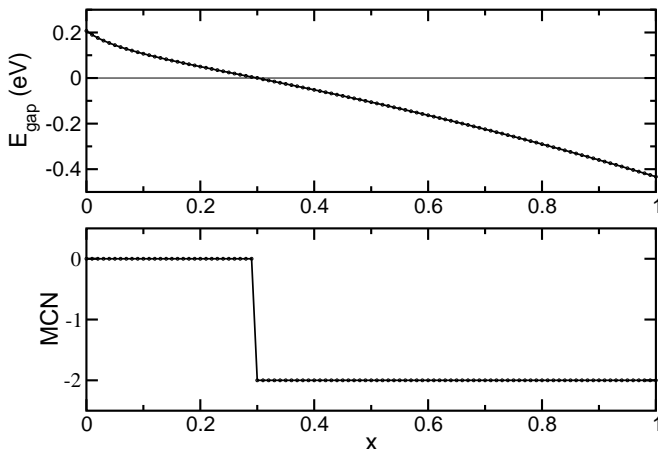


FIG. 3. Dependence of (a) the energy gap at the  $L$  point and (b) the Mirror Chern Number on the Sn content  $x$  for  $\text{Pb}_{1-x}\text{Sn}_x\text{Te}$  in the VCA.

### B. $\text{Pb}_{1-x}\text{Sn}_x\text{Te}$ in the Virtual Crystal Approximation

Our LDA calculations for PbTe and SnTe give two sets of the corresponding TBA parameters. Taking their composition weighted averages we obtain the TBA parameters for  $\text{Pb}_{1-x}\text{Sn}_x\text{Te}$  in the VCA. For Sn, we use pseudopotentials generated by us with 4 valence electrons. In Fig. 3 we show both the  $E_{gap}$  at the  $L$  point and the MCN as the functions of composition. As in the case of PbTe, where a sharp transition between trivial and nontrivial topological phases takes place at a well defined value of the lattice constant, in the case of  $\text{Pb}_{1-x}\text{Sn}_x\text{Te}$  a sharp transition takes place at the well defined Sn content. This is in contrast to the more realistic models of  $\text{Pb}_{1-x}\text{Sn}_x\text{Te}$  considered in the next Section.

## IV. MIXED $\text{Pb}_{1-x}\text{Sn}_x\text{Te}$ CRYSTALS

### A. Topological properties of band structures

We now turn to calculations, in which the two cations, Pb and Sn, are explicitly distinct.

We start with the simplest case of the  $1 \times 1 \times 1$  supercell  $\text{Pb}_3\text{Sn}_1\text{Te}_4$  containing eight atoms. As it turns out, most of the features characterizing larger supercells, with different numbers of Sn atoms and arbitrary spatial distribution of cations, are observed already for this case.

Energy gaps of PbTe are located at the four nonequivalent  $L$  points of the BZ,  $L = \frac{\pi}{a}(\pm 1, \pm 1, 1)$  or, in the case of SnTe, near these points. The Brillouin zones of supercells are "folded" relative to that of for pure PbTe, and in the literature their high symmetry points are denoted by various symbols.

Here, we denote by  $L_{gap}$  the point where for pure PbTe, the direct energy gap is the smallest. The coordinates

these  $L_{gap}$  points depend on the supercell. For example for  $1 \times 1 \times 1$  supercell  $L_{gap} = \frac{\pi}{a}(1, 1, 1)$ , for  $1 \times 1 \times 2$  supercell considered later,  $L_{gap} = \frac{\pi}{a}(1, 1, 0)$ , where  $a$  denotes lattice constant of the fcc lattice. The  $\Gamma$  point always corresponds to  $\mathbf{k} = 0$ .

In Fig. 4 we compare the band structures of  $\text{Pb}_4\text{Te}_4$  (left column) and of  $\text{Pb}_3\text{Sn}_1\text{Te}_4$  (right column) for topologically trivial (upper row) and nontrivial (lower row) cases. Only the highest eight valence bands and the lowest eight conduction bands are shown. The calculations are performed for lattice constants shown in the panels, where

$$a_0(x) = (6.46 - 0.16x) \text{ \AA} \quad (20)$$

is the equilibrium lattice constant according to the Vegard's law for  $\text{Pb}_{1-x}\text{Sn}_x\text{Te}$ .

The most important modification of the band structure relative to the VCA and caused by the distinction of the Pb and Sn atom is the splitting of levels. We stress that this splitting is not related to a change of the crystal point symmetry, which is  $O_h$  for both PbTe and  $\text{Pb}_3\text{Sn}_1\text{Te}_4$ , but to the chemical difference between Pb and Sn.

A closer inspection of the data in the lower right panel of the figure shows that for small lattice constants the main energy gap is shifted away from the  $L_{gap}$  point, as in SnTe at equilibrium.<sup>1,2</sup> When the lattice constant decreases this gap also closes, independently of the gap at the  $L_{gap}$  point what leads to the changes in the topological characteristics of the band structure. For  $\text{Pb}_3\text{Sn}_1\text{Te}_4$  the transition occurs for  $a/a_0(x) \approx 0.9897$  and for  $\mathbf{k} \approx 0.482 \times \frac{\pi}{a}(1, 1, 1)$ .

The pressure dependencies of the band energies at  $L_{gap}$  are shown in Fig. 5 for the eight highest valence bands and the eight lowest conduction bands. The results for  $\text{Pb}_3\text{Sn}_1\text{Te}_4$  (right panel) are compared with those for  $\text{Pb}_4\text{Te}_4$  (left panel). These sixteen bands are occupied by eight electrons. In PbTe, the band inversion occurs at  $a/a_0 = 0.97$ , and for smaller  $a$  electrons occupy cation rather than anion orbitals. In the case of  $\text{Pb}_3\text{Sn}_1\text{Te}_4$  the situation is more complicated. As it follows from Fig. 5, there is a large interval of  $0.97 < a/a_0(x) < 1.02$ , in which the band gap vanishes, i.e., the system is metallic, and electrons occupy combinations of the cation and anion  $p$  orbitals. Finally, for  $a < 0.97$ , the band gap is finite, the system is insulating, the band structure is inverted, and electrons occupy the cation orbitals only. In Fig. 6 we show energy gaps, contributions of  $p$  orbitals of different atoms to the wave functions of the top valence band at  $L_{gap}$ , and the MCN for the valence bands as a function of the lattice constant. The value of  $E_{gap}$  at  $L_{gap}$  follows from the behavior of the energy levels, Fig. 5. In addition to  $C_{Te}$ , we also show the contribution of cation  $p$  orbitals to the wave function. Because the considered supercell has the  $O_h$  point symmetry, it is possible to calculate the MCN. For  $a/a_0 > 1.02$  MCN=0, and when  $E_{gap} = 0$  we observe a jump to MCN=1. The interesting jump to MCN=-3 is related to the closing of the gap at a certain point along  $\Gamma \rightarrow L_{gap}$  direction, discussed

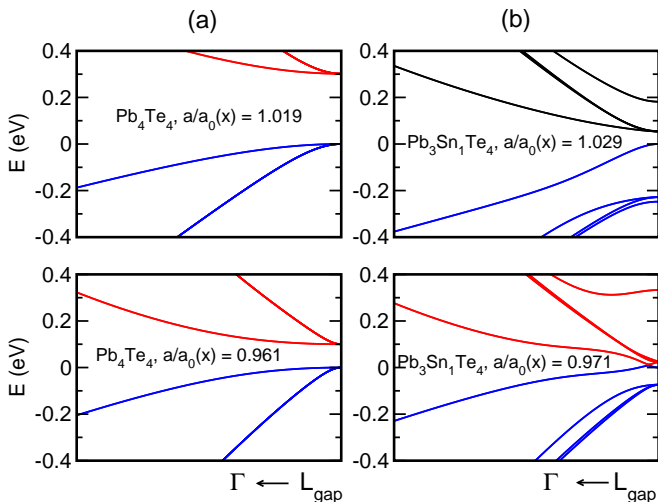


FIG. 4. (color online) Band structures of  $\text{Pb}_4\text{Te}_4$  (a) and of  $\text{Pb}_3\text{Sn}_1\text{Te}_4$  (b) for topologically trivial (upper row) and nontrivial (lower row) cases.

above, what evidently leads to the change of topological properties of the valence band structure. Finally, when  $a/a_0 < 0.97$ , then  $E_{gap}$  is negative, the valence band at the  $L_{gap}$  point is composed mainly from  $p(\text{Sn})$  orbitals, and  $\text{MCN}=-2$  like in the case of pure  $\text{SnTe}$ .

It turns out that this picture is very general. The behavior of the energy levels shown in Fig. 5 is qualitatively very similar for larger supercells with 16, 64, 216 atoms containing different numbers of randomly distributed Sn atoms. The main difference is that the degeneracy of levels is reduced not only by the presence of two types of cations, but also by the reduction of the crystal point symmetry for typical atomic configurations. We calculated the band structure characteristics for all nonequivalent atomic configurations for the 16-atom  $1 \times 1 \times 2$  supercell. (For larger supercells, the SCN were not calculated because they require non practically long computation times necessary to obtain convergent results.) As an example, in Fig. 7 we show the results for the  $1 \times 1 \times 2$  supercell with three Sn atoms. In the interval  $0.97 < a/a_0(x) < 1.03$  the energy gap is zero, and the anion and cation energy levels are mixed up, what is reflected in the abrupt variations of the band structure topology characterized by the SCN.

The conclusions from calculations for  $1 \times 1 \times 2$  supercell are as follows.

First, independent of the alloy composition (i.e., of number of cations in the supercell) and the spatial distribution of cations we always find a finite interval of the lattice constants in which  $E_{gap} = 0$ .

Second, when the energy gap closes we observe the abrupt drop in the values of  $C_{Te}$  from  $\sim 1.5$  to almost zero.

Third, for a given plane in the BZ the SCNs or MCNs

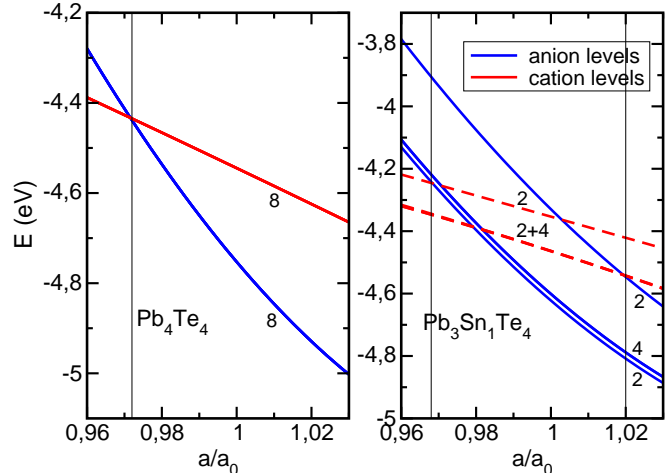


FIG. 5. (color online) Energy levels of the eight highest valence bands and the eight lowest conduction bands at the  $L$  point of the Brillouin zone. The continuous and broken lines correspond to levels which wave functions are built mainly from  $p$  orbitals of anions and cations, respectively. The numbers near the lines give the degeneracy of the levels (2+4 means that we have two lines, invisible in this scale, with the degeneracies 2 and 4, respectively). The thin vertical lines are the borders between topologically nontrivial, transition and topologically trivial regions of the lattice constant. Notice that for  $\text{Pb}_4\text{Te}_4$  the width of the transition region is zero.

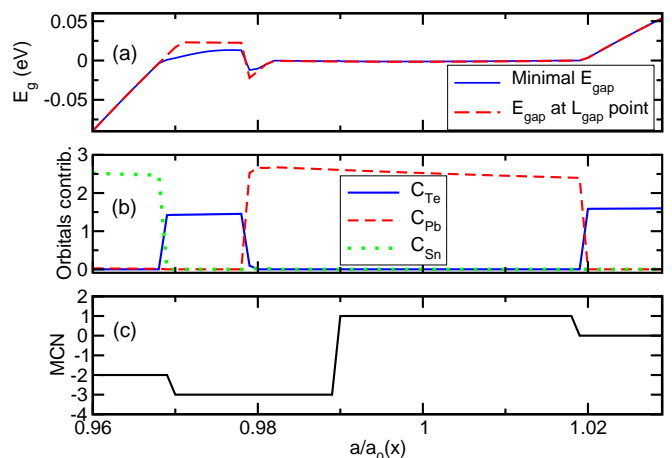


FIG. 6. (color online) Band structure characteristics of  $\text{Pb}_3\text{Sn}_1\text{Te}_4$ . Dependence on the lattice constant of: (a) Minimal energy gap along  $\Gamma \rightarrow L_{gap}$  direction and  $E_{gap}$  at the  $L_{gap}$ , (b) Contributions of pseudoatomic  $p$  orbitals to the valence band wave functions at  $L_{gap}$ , and (c) the Mirror Chern Number for valence bands.

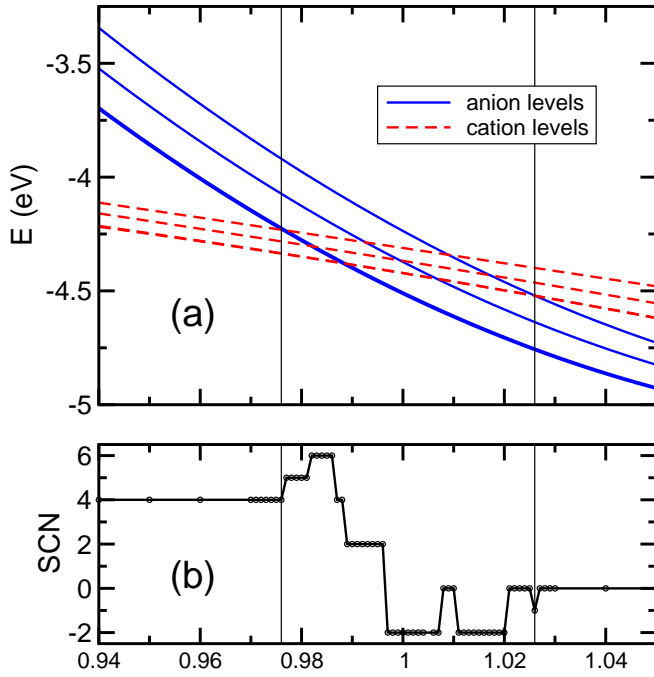


FIG. 7. (color online) Band energy levels at the  $L_{gap}$  point for anions and cations a) and the Spin Chern Number b) as the functions of the lattice constant for one of the configurations for 16-atom supercell containing three Sn atoms. The thin vertical lines are the borders between topologically nontrivial, transition and topologically trivial regions of the lattice constant.

do not uniquely characterize the topology of the band structure. In most cases, when the gap closes with the decreasing lattice constant, we observe a jump in SCN from zero to a nonzero value. However this is not always the case. For example, for  $1 \times 1 \times 2$  supercell containing two Sn atoms placed in such a way that they constitute a BCC lattice, the SCN does not change from the zero value when the gap closes. The same situation is found for MCN with respect to the (110) plane. Only for the MCN for the (001) plane, when the gap closes, we observe a jump to the value -2.

Finally, for many of the considered configurations, we observe a number of jumps of SCN in the topologically nontrivial region of  $a/a_0(x)$ . This confirms that, what is obvious from the mathematical point of view, the topological characteristics based on Chern numbers do not uniquely characterize the valence band vector bundles. In general, the topological indices based on Chern numbers may distinguish two phases when the values of these numbers are different, but if the values are the same it is impossible to decide whether the studied phases are different or not.

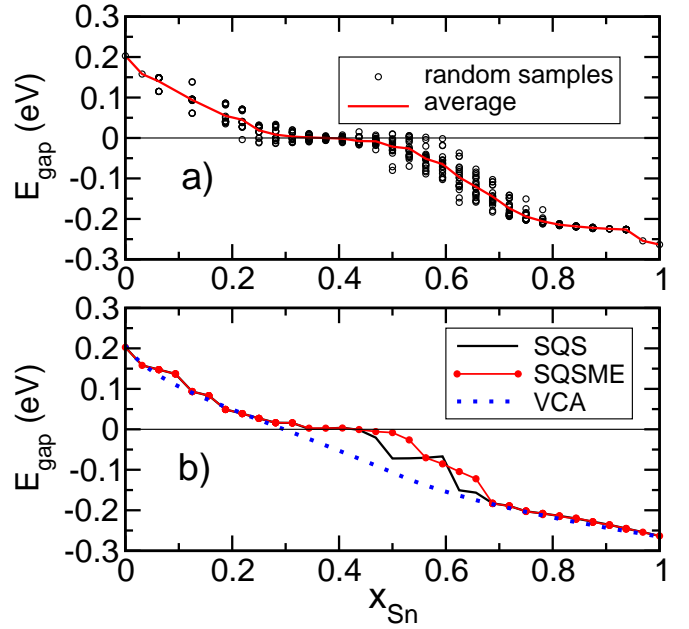


FIG. 8. (color online) (a) Minimal energy gaps on [111] direction for 20 randomly chosen tin configurations (points) and the average (solid line). (b) Minimal energy gaps on [111] direction for the best SQS tin configurations (solid line), for the configurations of minimal energies chosen from 10 best SQS (line with points) and for the VCA (dotted line).

## B. Composition dependence of $\text{Pb}_{1-x}\text{Sn}_x\text{Te}$ band gap

The calculated composition dependence of the  $\text{Pb}_{1-x}\text{Sn}_x\text{Te}$  band gap is shown in Fig. 8. The results were obtained using three approaches, namely by averaging over 20 different random distributions of cations in the supercell, the Special Quasirandom Structures (SQS) method,<sup>15</sup> and the VCA.

The  $2 \times 2 \times 2$  supercells containing 64 atoms allow us to study energy gaps for a dense set of 32 compositions. For each composition, 20 random cation configurations were considered. In Fig. 8a we show minimal energy gaps along the [111] direction. The first observation to make is that, for a given number of Sn/Pb atoms, the band gaps strongly depend on their distribution in the supercell. Indeed, the spread of  $E_{gap}$  can be as high as 0.15 eV, which is close to the band gap itself. However, for some composition ranges, especially for  $x < 0.2$  and  $x > 0.8$ , several configurations give almost the same  $E_{gap}$ . (We do not have a convincing explanation of this effect.)

Secondly, in spite of the large fluctuations, the gap averaged over the configurations,  $E_{gap}^{ave}$ , is a smooth function of composition. The composition dependence of  $E_{gap}^{ave}$  is strongly non-linear, but the non-linearity does not consist in the typical parabolic bowing, which characterizes most of semiconductor alloys. The most prominent feature is that  $E_{gap}^{ave}$  vanishes to within 0.01 eV in a wide composition range  $0.3 < x < 0.45$ . This effect can be

explained based on the previous discussion of the energy levels splitting due to the presence of two different cations in the alloy.

Because our simple averaging procedure of  $E_{gap}$  has no solid physical foundation, we calculated the band gap  $E_{gap}^{SQS}$  for  $Pb_{1-x}Sn_xTe$  using the SQS method. In this approach, one approximates a real random alloy without the translational symmetry by a periodic structure of the same composition chosen in such a way that certain parameter  $\epsilon$ , a measure describing the difference between the atomic spatial distribution of this structure and of perfectly random system is minimized. In order to obtain best SQSs we proceeded along the prescription described in Ref. 20 where the parameter  $\epsilon$  is defined. The results for energy gaps obtained for our best SQSs for even number of tin atoms in the supercells are identical to those calculated using the Table 1 in Ref. 20.

The SQS energy gaps  $E_{gap}^{SQS}$  are shown in Fig. 8b by the continuous line. The overall composition dependence of the  $E_{gap}^{SQS}$  is quite close to the average  $E_{gap}^{ave}$  shown in Fig. 8a. In particular,  $E_{gap}^{SQS} = 0$  in the same composition interval  $0.35 < x < 0.45$ . (We note that  $E_{gap}^{SQS}$  is constant for  $0.5 < x < 0.6$ , but this seems to be an artifact of the method.) The SQS results of Fig. 8b are qualitatively similar to those obtained in Ref. 21 where this problem was considered, although for smaller systems.

During the crystal growth there are two factors which decide about the placements of different cations in the crystal lattice. The first one is the configurational entropy, which promotes the alloy randomness, and the second factor is the total energy, which tends to assume a minimal value, which can result in alloy ordering or phase segregation. Although due to high temperature of the crystal growth and the finite time of the process it seems that the entropy factor is the most important one, however the second one should not be totally neglected. By construction, the SQS method takes into account only the entropy factor. In order to study the influence of the energy factor, instead of taking the best SQS configuration characterized by the smallest value of  $\epsilon$ , from about 300 000 configurations generated during the program's run we chose 10 configurations characterized by smallest values of  $\epsilon$ . For a given tin's concentration the dispersion of  $\epsilon$ s for these 10 configurations was very small. The dispersion of energies depend on tin's concentration. For  $x < 0.3$  and for  $x > 0.7$  it is negligible, however, for  $0.3 < x < 0.7$  the difference between the total energies for configurations with highest and lowest total energies is in the interval 0.001 – 0.12 eV. Taking for the band structure calculations the configuration of the lowest energy we obtain the SQSME (special quasirandom structure minimal energy) curve in Fig. 8b. Although this curve is not perfectly smooth, the step-like behavior for  $0.5 < x < 0.6$  of the SQS curve disappears.

For comparison, in Fig. 8b we also show the predictions of VCA (dotted line). It is clear that the VCA fails in describing the band gap of  $Pb_{1-x}Sn_xTe$  for a relatively wide range of compositions, in which the transition from

the direct to the inverted band structure, or, in other words, from the topologically trivial to non-trivial situation takes place.

We see that SQS and SQSME results practically coincide for most compositions except the small composition window  $0.5 < x < 0.65$ , where the smooth SQSME data seem to be more physical. Let us notice that the average band gap  $E_{gap}^{ave}(x)$  shown in Fig. 8a is also close to that obtained within the SQS/SQSME method. All these approaches explicitly differentiate between the two kinds of cations, Sn and Pb. On the other hand, the VCA assumes an averaged cation, and neglects the effect of fluctuations.

While the SQS method is a well justified procedure, our analysis of the gap for various configurations, Fig. 8a, provide a deeper insight into the problem by showing the considerable impact of fluctuations of both composition and configurations. As a consequence, the spread in  $E_{gap}$  shows that local composition fluctuations can result in efficient alloy scattering of carriers, which implies shortening of carrier lifetime.

## V. CONCLUSIONS

We analyzed topological properties of the mixed  $Pb_{1-x}Sn_xTe$  crystals. Three approaches were used to calculate band structure, namely the virtual crystal approximation, the supercell method, and the special quasirandom structures method. The transition between the trivial and non-trivial topological phase can be driven either by the increasing content of Sn in  $Pb_{1-x}Sn_xTe$  or by hydrostatic pressure for  $x < 0.3$ , when the band gap at ambient pressure is positive. From our results the following conclusions may be drawn.

1. For a compound crystalline semiconductors like PbTe, the transition from the trivial to the non-trivial topological phases is sharp and driven by the pressure-induced inversion of the band gap character. A sharp transition is predicted also for  $Pb_{1-x}Sn_xTe$  mixed crystals at  $x \approx 0.3$ , but only when the VCA is used.

2. Both the supercell method and the SQS approach explicitly differentiate between the two cations, Pb and Sn in  $Pb_{1-x}Sn_xTe$ . This induces additional splittings of the energy bands, which are caused by different potentials of Pb and Sn and by the reduction of the crystal symmetry. In consequence, transitions from the trivial to the non-trivial phase are broad. The composition ranges in which the band structure is direct ( $0 < x < 0.3$ ) and inverted ( $0.6 < x < 1$ ) are separated by an unexpectedly large window  $0.3 < x < 0.6$  characterized by the vanishing band gap. Similarly, the pressure induced phase transition is broad, and extends over a window of 2 % of the lattice constant values, in which  $E_{gap} \approx 0$ . This shows that the sharpness of topological transitions predicted by the VCA is an artifact.

3. In the regions of the compositions or of the lattice constants with the vanishing band gap, there is no

criterion to decide whether the topological phase is trivial or nontrivial, because the mirror Chern number, the spin Chern number, and the orbital content of band edge wave functions vary rapidly and randomly. In this interval, topology of the band structure is very complicated, and sometimes the topological indices or the orbital content of the wave functions suggest triviality of the phase. To establish the phase, it is necessary to analyze the band structure in a larger interval of the lattice constants.

4. Our results can explain the experimental studies of conductivity of  $\text{Pb}_{1-x}\text{Sn}_x\text{Te}$  with  $x = 0.25$  reported recently in Ref. 22. The authors observe a pressure-driven transition from the insulating to the metallic phase at about 12 kbar, followed by the re-entrance of the insulating phase at 24 kbar. According to Fig. 8,  $\text{Pb}_{1-x}\text{Sn}_x\text{Te}$  with  $x = 0.25$  has a direct band structure with a positive band gap of about 0.05 eV. Analysing the energy gap dependence on the lattice parameter for 64 atom supercell containing 25% of tin with SQS distribution of cations and knowing that  $dE_{gap}/dp=70$  meV/GPa<sup>1,2</sup> it is possible to predict that the band gap, with the increasing hydrostatic pressure, closes at about 2 kbar and  $\text{Pb}_{1-x}\text{Sn}_x\text{Te}$  is metallic up to 16 kbar. For higher pressures  $E_{gap} < 0$ , and the alloy is insulating. Com-

paring those results with experiment we observe that the predicted transition pressure to the metallic phase is too low (which can be due to our inaccuracy in determining  $E_{gap}$ ), but the range of pressures corresponding to the gapless situation, 14 kbar, fits well the experimental value, 12 kbar.

5. Another experimental verification of our theoretical findings could be performed with low temperatures optical measurements in the THz range under hydrostatic pressure for crystals with low carrier concentrations. Although very challenging, such an experiment is feasible, as shown by pressure studies of infrared reflectivity in the closely related  $\text{Pb}_{1-x}\text{Sn}_x\text{Se}$  TCI mixed crystals.<sup>23</sup>

## ACKNOWLEDGMENTS

The authors acknowledges the support from NCN (Poland) research projects Nr. UMO-2016/23/B/ST3/03725 (AŁ) and Nr. UMO-2014/15/B/ST3/03833 (TS). The suggestions and discussions with Professor Ryszard Buczko are kindly acknowledged.

- 
- <sup>1</sup> G. Nimtz, and B. Schlicht, in: *Narrow-Gap Semiconductors* (ed. G. Höhler), Springer Tracts in Modern Physics, Vol. 98 (ed. G. Hohler) (Springer-Verlag, Berlin 1983).
- <sup>2</sup> D. R. Khoklov (ed.) *Lead Chalcogenides: Physics and Applications* (Taylor and Francis, New York 2003).
- <sup>3</sup> P. Dziawa, B. J. Kowalski, K. Dybko, R. Buczko, A. Szczerbakow, M. Szot, E. Łusakowska, T. Balasubramanian, B. M. Wojek, M. H. Berntsen, O. Tjernberg, and T. Story, *Nature Mat.* **11**, 1023 (2012).
- <sup>4</sup> Y. Tanaka, Z. Ren, T. Sato, K. Nakayama, S. Souma, T. Takahashi, K. Segawa, and Y. Ando, *Nat. Phys.* **8**, 800 (2012)
- <sup>5</sup> S.-Y. Xu, C. Liu, N. Alidoust, M. Neupane, D. Qian, I. Belopolski, J.D. Denlinger, Y.J. Wang, H. Lin, L.A. Wray, G. Landolt, B. Slomski, J.H. Dil, A. Marcinkova, E. Morosan, Q. Gibson, R. Sankar, F.C. Chou, R.J. Cava, A. Bansil, and M.Z. Hasan, *Nat. Commun.* **3**, 1192 (2012)
- <sup>6</sup> B. M. Wojek, P. Dziawa, B. J. Kowalski, A. Szczerbakow, A. M. Black-Schaffer, M. H. Berntsen, T. Balasubramanian, T. Story, and O. Tjernberg, *Phys. Rev. B* **90**, 161202(R) (2014)
- <sup>7</sup> P. Barone, T. Rauch, D. Di Sante, J. Henk, I. Mertig, and S. Picozzi, *Phys. Rev. B* **88**, 045207 (2013)
- <sup>8</sup> B. M. Wojek, R. Buczko, S. Safaei, P. Dziawa, B. J. Kowalski, M. H. Berntsen, T. Balasubramanian, M. Leandersson, A. Szczerbakow, P. Kacman, T. Story, and O. Tjernberg, *Phys. Rev. B* **87**, 115106 (2013)
- <sup>9</sup> S. Safaei, P. Kacman, and R. Buczko, *Phys. Rev. B* **88**, 045305 (2013)
- <sup>10</sup> S. Safaei, M. Galicka, P. Kacman, and R. Buczko, *New J. Phys.* **17**, 063041 (2015)
- <sup>11</sup> T. H. Hsieh, H. Lin, J. Liu, W. Duan, A. Bansil, and L. Fu, *Nature Comm.* **3**, 982 (2012).
- <sup>12</sup> L. Fu, and C. L. Kane, *Phys. Rev. Lett.* **109**, 246605 (2012)
- <sup>13</sup> E. Prodan, *Phys. Rev. B* **80**, 125327 (2009)
- <sup>14</sup> A. Łusakowski 46<sup>th</sup> International School & Conference on the Physics of Semiconductors, "Jaszowiec 2017", unpublished
- <sup>15</sup> A. Zunger, S.-H. Wei, L. G. Ferreira, and J. E. Bernard, *Phys. Rev. Lett.* **65**, 353 (1990)
- <sup>16</sup> see <http://www.openmx-square.org>
- <sup>17</sup> D. M. Ceperley, and B. J. Alder, *Phys. Rev. Lett.* **45**, 566 (1980).
- <sup>18</sup> A. Łusakowski, P. Bogusławski, and T. Radzyński, *Phys. Rev. B* **83**, 115206 (2011)
- <sup>19</sup> T. Fukui, Y. Hatsugai, and H. Suzuki, *J. Phys. Soc. Jpn.* **74**, 1674 (2005)
- <sup>20</sup> J. von Pezold, A. Dick, M. Friák, and J. Neugebauer, *Phys. Rev. B* **81**, 094203 (2010)
- <sup>21</sup> X. Gao, and M. S. Daw, *Phys. Rev. B* **77**, 033103 (2008)
- <sup>22</sup> T. Liang, S. Kushwaha, J. Kim, Q. Gibson, J. Lin, N. Kioussis, R. J. Cava, and N. P. Ong, *Sci. Adv.* **3**, e1602510 (2017)
- <sup>23</sup> X. Xi, X.-G. He, F. Guan, Z. Liu, R. D. Zhong, J. A. Schneeloch, T. S. Liu, G. D. Gu, X. Du, Z. Chen, X. G. Hong, W. Ku, and G. L. Carr, *Phys. Rev. Lett.* **113**, 096401 (2014).